Photoelectrochemical Properties of Fe_2O_3−Nb_2O_5 Films Prepared by Sol−Gel Method

Hidekazu Miyake and Hiromitsu Kozuka*

Department of Materials Science and Engineering, Kansai University, 3-3-35 Yamate-cho, Suita 564-8680, Japan

Received: February 16, 2005; In Final Form: June 16, 2005

Fe_2O_3−Nb_2O_5 coating films of various Nb/(Fe + Nb) mole ratios were prepared on nesa silica glass substrates from $Fe(NO_3)_3$·$9H_2O$ − $NbCl_5$ − $CH_3(CH_2)_2CH_2OH$ − CH_3COOH solutions by the sol−gel method. The photoanodic properties were studied in a three-electrode cell with an aqueous buffer solution of pH = 7 as the supporting electrolyte. The crystalline phases identified were α-Fe_2O_3 (Nb/(Fe + Nb) = 0), α-Fe_2O_3 + $FeNbO_4$ (Nb/(Fe + Nb) = 0.25), $FeNbO_4$ (Nb/(Fe + Nb) = 0.5), $FeNbO_4$ + Nb_2O_5 (Nb/(Fe + Nb) = 0.75), and Nb_2O_5 (Nb/(Fe + Nb) = 1). When the Nb/(Fe + Nb) mole ratio increased from 0 to 0.25, the crystalline phases changed from α-Fe_2O_3 to α-Fe_2O_3 + $FeNbO_4$, the photoanodic current under white light illumination increased, and the photoanodic current under monochromatized light illumination increased in both visible and ultraviolet regions. When the Nb/(Fe + Nb) ratio increased over 0.25, the crystalline phases changed to $FeNbO_4$, $FeNbO_4$ + Nb_2O_5, or Nb_2O_5, and the photoanodic current decreased. The sample consisting of α-Fe_2O_3 and $FeNbO_4$ (Nb/(Fe + Nb) = 0.25) exhibited photoresponse extending to 600 nm and an IPCE of 18% at a wavelength of 325 nm.

1. Introduction

A number of studies have been carried out on wet-type solar cells since the discovery of the Honda−Fujishima effect.[1] Semiconductor electrodes for wet-type solar cells need to have high energy conversion efficiency and high photoelectrochemical stability in aqueous solutions. Despite the photochemical stability in aqueous solutions, TiO_2 has a large band gap of about 3 eV and hence is photoexcited only by UV light, which occupies only 5% of the solar spectra. Therefore, semiconductor electrodes that exhibit photoresponse to the visible light are strongly demanded.

α-Fe_2O_3, an n-type semiconductor, is another photoelectrode material for wet-type solar cells that has been studied for a long time.[2−7] α-Fe_2O_3 has a relatively small band gap of ca. 2.2 eV and is photoelectrochemically stable in aqueous solutions. However, because of the small optical absorption coefficient and small carrier mobility, α-Fe_2O_3 normally shows low quantum efficiency.[6]

Recently, our group prepared Fe_2O_3−TiO_2 ceramic thin films by the sol−gel method.[8] The photoanodic properties were studied in a three-electrode cell with an aqueous buffer solution of pH = 7 as the supporting electrolyte. The effects of the Ti/(Fe + Ti) mole ratio were studied on the photoanodic properties. As a result, though pure TiO_2 had the maximum IPCE (incident photon to current efficiency) in the UV range, the film prepared from the solution of Ti/(Fe + Ti) = 0.2 showed maximum IPCE in the visible range of 350−550 nm. In addition, when poly(vinylpyrrolidone) (PVP) was added in the coating solution, IPCE increased in the UV and visible range, achieving 32% and 22% at the wavelengths of 325 and 400 nm, respectively.

Since the crystalline phases of the film prepared from the solution of Ti/(Fe + Ti) = 0.2 without PVP were α-Fe_2O_3 and Fe_2TiO_5, it was thought that the increase in IPCE in the visible range results from the coexistence of two phases in nanoscale. However, the direct band gap of the film was equal to that of α-Fe_2O_3, and the Ti/(Fe + Ti) film prepared with PVP was single-phase α-Fe_2O_3. Also, the donor density of the film with Ti/(Fe + Ti) = 0.2 was the maximum, 2 orders of magnitude higher than that of the films with other Ti/(Fe + Ti) ratios. Therefore, it was thought that the increase in donor density, which results from doping α-Fe_2O_3 with Ti^{4+}, causes the decrease in resistivity of the films, which leads to the increase in IPCE.

If the increase in donor density by the doping truly leads to the increase in IPCE in the visible range, it would be possible that IPCE in the visible range is increased by doping α-Fe_2O_3 with Nb^{5+}, which has higher valence than Ti^{4+}. Nb^{5+} is also common to Ti^{4+} in terms of having no d electrons. In the present study, with expectation of an increase in IPCE by doping α-Fe_2O_3 with Nb^{5+}, Fe_2O_3−Nb_2O_5 films were prepared from solutions of various Nb/(Fe + Nb) ratios, and the effect of the Nb/(Fe + Nb) ratio on photoelectrochemical properties was studied.

TABLE 1: Compositions of the Starting Solutions

	mole ratio			
solution	$Fe(NO_3)_3$·$9H_2O$	$NbCl_5$	CH_3COOH	$CH_3(CH_2)_2CH_2OH$
Nb0	1	0	1	80
Nb0.25	0.75	0.25	1	80
Nb0.5	0.5	0.5	1	80
Nb0.75	0.25	0.75	1	80
Nb1	0	1	1	80

2. Experimental Section

2.1. Preparation. $Fe(NO_3)_3$·$9H_2O$, $NbCl_5$, $CH_3(CH_2)_2CH_2OH$, and CH_3COOH, all purchased from Wako Pure Chemical Industries, Osaka, Japan, were used as the starting materials. The solutions of compositions given in Table 1 were prepared. CH_3COOH was added to $CH_3(CH_2)_2CH_2OH$ in the ambient atmosphere, and $NbCl_5$ and $Fe(NO_3)_3$·$9H_2O$ were dissolved in the resultant solution in flowing N_2 gas. The solutions thus obtained were concentrated using a rotary pump until the total volume of the solutions were reduced from 30 to 20 mL. The resultant homogeneous solutions were used as coating solutions.

10.1021/jp058051b CCC: $30.25
Published on Web 09/03/2005

Gel films were deposited on silica glass substrates coated with nesa (Sb-doped SnO_2), where dip-coating was conducted at a substrate withdrawal speed of 3 cm·min^{-1}. The gel films were fired at 600−800 °C for 10 min. Gel film deposition and heat treatment were repeated three times, and the resultant films were used as samples.

2.2. Characterization. The thicknesses of the films prepared by one-time deposition were measured using a contact probe surface profilometer (SE3400, Kosaka Laboratory, Tokyo, Japan). For the measurement of the film thickness, a part of the gel film was scraped off with a surgical knife before heat treatment, and the thickness was determined from the level difference between the coated and the scraped parts after heat treatment.

The crystalline phases of the films were identified by X-ray diffraction measurement (XRD) using an X-ray diffractometer (RAD IIA, Rigaku, Osaka, Japan) with a thin-film attachment at an incident angle of 1°. The X-ray source used was Cu Kα radiation operated at 40 kV and 40 mA. Electron microscopic observation was made using a field emission type scanning electron microscope, FE-SEM (JSM-6500F, JEOL, Tokyo, Japan). Optical absorption spectra were measured on the film samples using an optical spectrometer (UV-2400PC, Shimadzu, Kyoto, Japan), where a bare nesa silica glass substrate was used as the reference.

2.3. Measurement of the Photoanodic Properties. Photoanodic properties of the films were evaluated in a three-electrode cell using a potentiostat (HZ3000, Hokuto Denko, Osaka, Japan) consisting of the film electrode sample, a platinized Pt electrode, and an SCE as the working, counter, and reference electrodes, respectively, and of a buffer solution of pH 7, an aqueous solution of 0.2 M $Na_2B_4O_7$, 0.14 M H_2SO_4, and 0.3 M Na_2SO_4, as the supporting electrolyte.

For measuring the current−potential curves, the potential of the working electrode was scanned from 0 to 1.5 V vs saturated calomel electrode (SCE) at a rate of 20 mV·s^{-1}. A 500-W xenon lamp (model UXL-500-D-0, XB-50101AA-A, UI-502Q, Ushio Denki, Tokyo, Japan) was used as the light source where the light intensity was reduced to 3 W at a wavelength of 500 nm using ND filters.

Action spectra of the films were measured at 1 V vs SCE, where the xenon lamp light was monochromatized using a monochromator (SPG-100, Shimadzu, Kyoto, Japan). The intensity of the monochromatized light was measured using a power meter (TQ8210, TQ82107, Advantest, Tokyo, Japan, and NOVA, PD300-UV, Ophir Japan, Saitama, Japan), which was ca. 22 μW at a wavelength of 500 nm. For this measurement, the film was first illuminated for 10 s, and then, the light was turned off. The difference in current before and after turning off the light was taken as the photocurrent. Quantum efficiency, IPCE, was calculated from photocurrent and incident light intensity.

Space charge capacity, C, was evaluated at a frequency of 1 kHz and at various electrode potentials, V, using the potentiostat and a frequency response analyzer (model FRA-5020, NF Elecronic Instruments, Kanagawa, Japan). A Mott−Schottky plot was made, i.e., C^{2-} was plotted against $V - V_{fb}$, where V_{fb} is the flat band potential of the film electrode.

3. Results

3.1. Effect of the Nb/(Fe + Nb) Ratio. *3.1.1. Film Thickness, Crystalline Phases, and Microstructure of the Films.* Film electrode samples were prepared from the solutions of various Nb/(Fe + Nb) ratios. The gel films were fired at 700 °C where gel film deposition and heat treatment were repeated three times. Hereafter, the thin-film sample prepared from the solution of Nb/(Fe + Nb) = 0.75, for example, is denoted as Nb0.75. The thicknesses of the films prepared from the solutions of Nb/(Fe + Nb) = 0−1 are shown in Table 2. Because the thickness of the films prepared with one-time coating ranged 14−30 nm, the thickness of the films prepared with three-times coating is estimated to be 42−90 nm.

TABLE 2: Thickness of the Films Prepared from the Solutions of Various Nb/(Fe + Nb) Mole Ratios via One-Time Coating and Heat Treatment at 700° C

solutions	thickness/nm
Nb0	18
Nb0.25	20
Nb0.5	30
Nb0.75	14
Nb1	20

Figure 1 shows the XRD patterns of the films thus obtained via three-times coating with firing at 700 °C. The diffraction peaks attributed to α-Fe_2O_3 were observed for Nb0, α-Fe_2O_3 and $FeNbO_4$ for Nb0.25, $FeNbO_4$ for Nb0.5, $FeNbO_4$ and Nb_2O_5 for Nb0.75, and Nb_2O_5 for Nb1.

Figure 2 shows the SEM images of the surface of the films. The grain size tended to increase with increasing Nb/(Fe + Nb) ratio, from ca. 50 to 150 nm, which, however, is the size of the secondary particles.

3.1.2. Optical Absorption Spectra. Figure 3 shows the optical absorption spectra of the films prepared via three-times coating with firing at 700 °C. For Nb0, the onset of absorption was seen around 580 nm (2.1 eV) and a broad peak around 400 nm (3.1 eV). The onset of absorption around 580 nm and the broad peak around 400 nm are attributed to the indirect transition and the direct transition corresponding to charge transfer from the O2p valence band to the Fe3d conduction band, respectively, of α-Fe_2O_3.[6] For Nb0.25, the onset of absorption was seen around 580 nm (2.1 eV) and 470 nm (2.6 eV) and for Nb0.5 around 470 nm (2.6 eV). The absorption onset around 470 nm for Nb0.25 and Nb0.5 is attributed to indirect transition in $FeNbO_4$.[9]

3.1.3. Current−Potential Curves. Figure 4 shows the current−potential curves of the films prepared via three-times coating with firing at 700 °C where the difference in current measured in light (the solid line) and dark (the broken line) is regarded as the photocurrent. When the Nb/(Fe + Nb) ratio

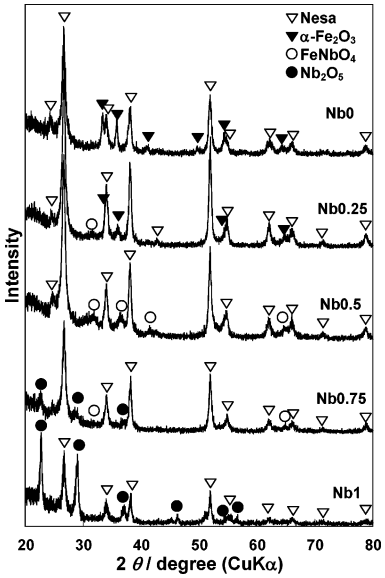

Figure 1. 1. XRD patterns of the film electrodes prepared from solutions of various Nb/(Fe + Nb) ratios via three-times coating with firing at 700 °C.

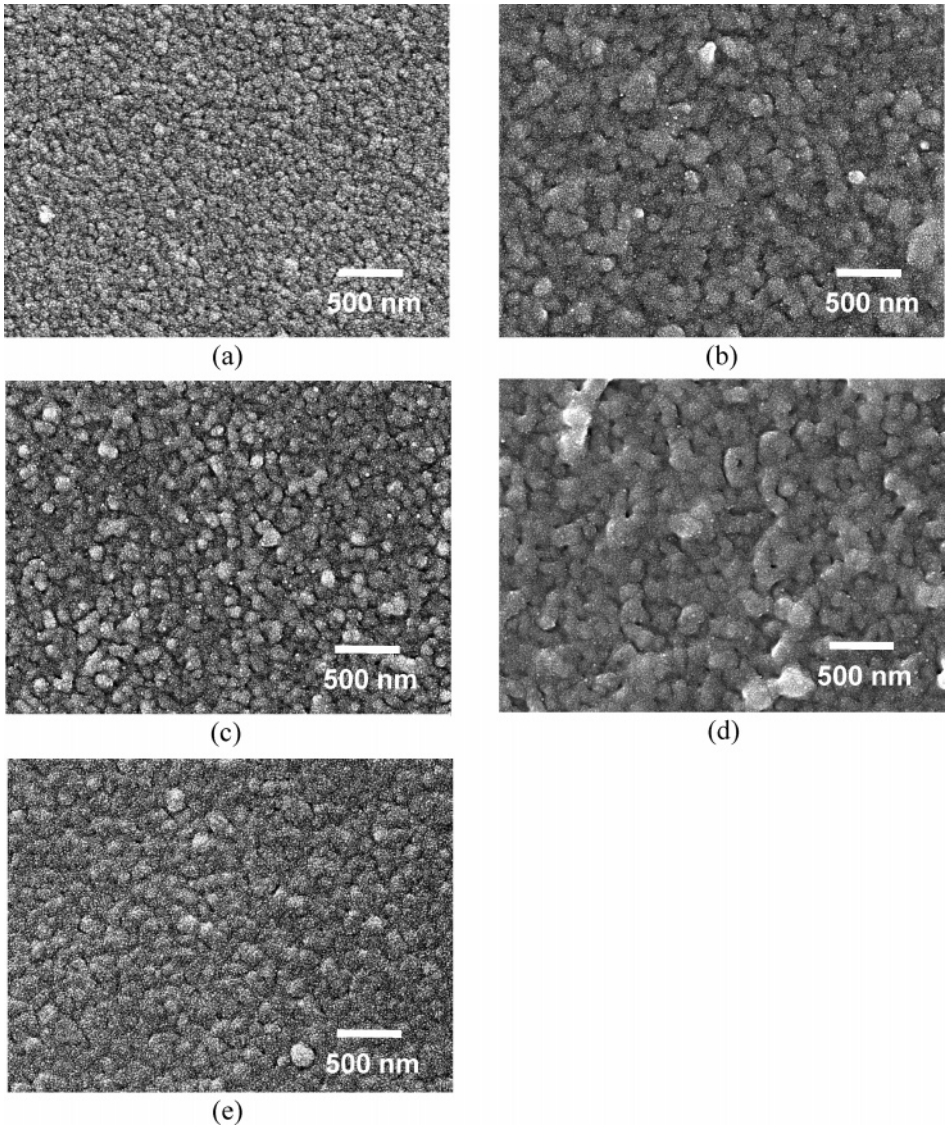

Figure 2. 2. SEM images of the surface of the film electrodes prepared from solutions with Nb/(Fe + Nb) ratios of (a) 0, (b) 0.25, (c) 0.5, (d) 0.75, and (e) 1 via three-times coating with firing at 700 °C.

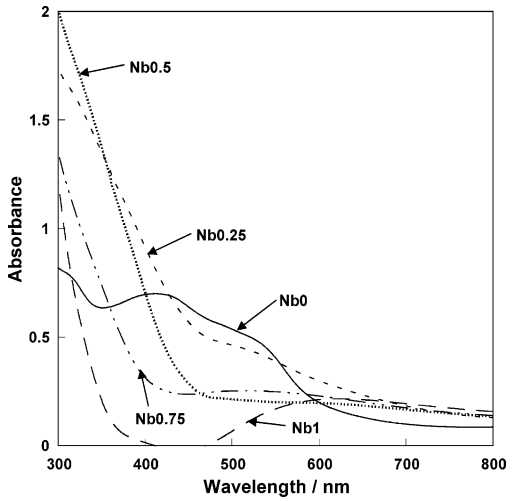

Figure 3. 3. Optical absorption spectra of the film electrodes prepared from solutions of various Nb/(Fe + Nb) ratios via three-times coating with firing at 700 °C.

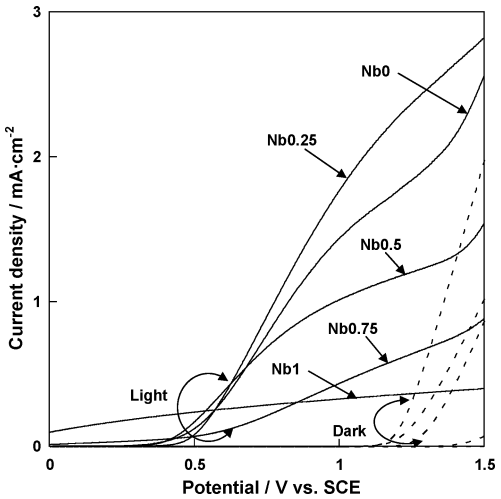

Figure 4. 4. Current−potential curves of the film electrodes prepared from solutions of various Nb/(Fe + Nb) ratios via three-times coating with firing at 700 °C.

increased from 0 to 0.25, the photocurrent increased. However, when the Nb/(Fe + Nb) ratio increased over 0.25, the photocurrent decreased with increasing Nb/(Fe + Nb) ratio.

3.1.4. Action Spectra. Figure 5 shows the action spectra of the films prepared via three-times coating with firing at 700 °C. The measurement was performed at a working electrode poten-

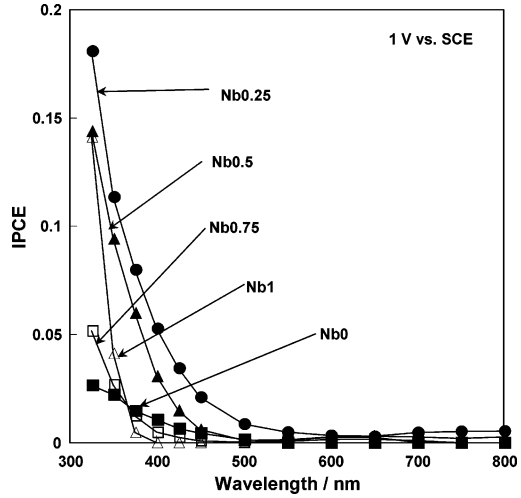

Figure 5. 5. Action spectra of the film electrodes prepared from solutions of various Nb/(Fe + Nb) ratios via three-times coating with firing at 700 °C. The measurement was conducted at 1.0 V vs SCE.

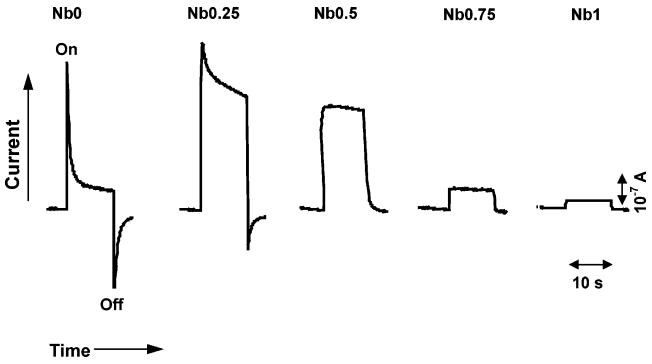

Figure 6. 6. Photocurrent transient curves of Nb0, Nb0.25, Nb0.5, Nb0.75, and Nb1 under irradiation with monochromatic light of a wavelength of 375 nm at 1.0 V vs SCE.

tial of 1.0 V vs SCE. As seen in the figure, when the Nb/(Fe + Nb) ratio increased from 0 to 0.25, IPCE at wavelengths of <600 nm increased. On the other hand, when the Nb/(Fe + Nb) ratio increased over 0.25, IPCE at wavelengths of 400−500 nm decreased. The photoresponse of Nb0.25 extended to longer wavelengths (600 nm) than the other samples, and IPCE at a wavelength of 400 nm was about 5%, reaching 18% at 325 nm.

Figure 6 shows the photocurrent transient response in light and dark for these films, where photocurrent was measured before and after illuminating the samples at 1.0 vs SCE with monochromatized light at a wavelength of 375 nm for 10 s. As seen in the figure, a spikelike transient response observed on illuminating and turning off the light decreased with increasing Nb/(Fe + Nb) ratio from 0 to 0.25 and disappeared over 0.5. The same behavior was observed at other wavelengths.

3.1.5. Mott−Schottky Plots. Figure 7 shows the Mott−Schottky plots of the films prepared via three-times coating with firing at 700 °C. The flat band potentials obtained from the intercept of the potential axis were −0.4, −0.3, −0.2, −0.3, and −0.6 V vs SCE for Nb0, Nb0.25, Nb0.5, Nb0.75, and Nb1, respectively, as summarized in Table 3. The donor density, N_d, was calculated from the slope of the plot using the Mott−Schottky equation

$$C^{2-} - \frac{2}{e\epsilon\epsilon_0 N_d}\left[(V - V_{fb}) - \frac{kT}{e}\right] \qquad (1)$$

where C is the space charge capacitance, ϵ the dielectric constant

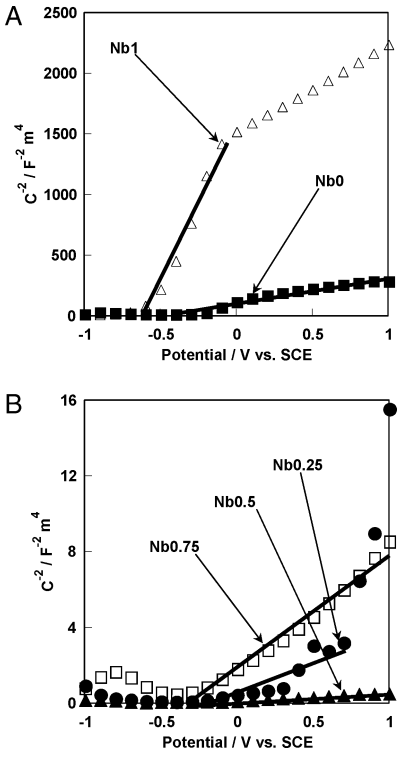

Figure 7. 7. Mott−Schottky plots of the film electrodes prepared from solutions of various Nb/(Fe + Nb) = (a) 0 and 1, and (b) 0.25, 0.5, and 0.75, via three-times coating with firing at 700 °C.

TABLE 3: Flat Band Potential V_{fb}, Donor Density N_d, and Width of the Space Charge Layer W of the Film Electrodes Prepared from the Solutions of Various Nb/(Fe + Nb) Mole Ratios via Three-Times Coating and Heat Treatment at 700 °C

solution	V_{fb}/V vs SCE	$N_d/10^{25}$ m^{-3}	W/nm
Nb0	−0.4	5.64[a]	16.5[a]
Nb0.25	−0.3	953[a]−8660[b]	0.14[b]−1.23[a]
Nb0.5	−0.2	3020[a]−27400[b]	0.22[b]−0.66[a]
Nb0.75	−0.3	224[a]−2040[b]	0.28[b]−2.52[a]
Nb1	−0.6	4.58[b]	6.52[a]

[a] Calculated on the assumption of $\epsilon = 100$ (Fe_2O_3). [b] Calculated on the assumption of $\epsilon = 11$ (Nb_2O_5).

of the film, ϵ_0 the dielectric constant of vacuum, V the applied potential, k Boltzmann's constant, and T the temperature. The width of the space charge layer, W, was calculated from N_d values obtained using eq 2

$$W = \left[\frac{2\epsilon\epsilon_0(V - V_{fb})}{eN_d}\right]^{1/2} \qquad (2)$$

where the dielectric constants ϵ of α-Fe_2O_3 and Nb_2O_5 were assumed to be 100[10] and 11,[11] respectively. W values for Nb0.25−Nb0.75 were calculated using ϵ values of both α-Fe_2O_3 and Nb_2O_5. N_d and W thus obtained are listed in Table 3 as well as V_{fb}. As shown in Table 3, the donor density once increased and then decreased, and correspondingly, the width of space charge layer once decreased and then increased with increasing Nb/(Fe + Nb) ratio.

3.2. Effect of the Heating Temperature. To investigate the effect of the heating temperature, the gel films were prepared from the solution of Nb/(Fe + Nb) = 0.25 and fired at 600, 700, or 800 °C for 10 min. The gel film deposition and heat treatment were repeated three times.

Figure 8 shows the XRD patterns of the films thus obtained. The diffraction peaks attributed to α-Fe_2O_3 and $FeNbO_4$ were

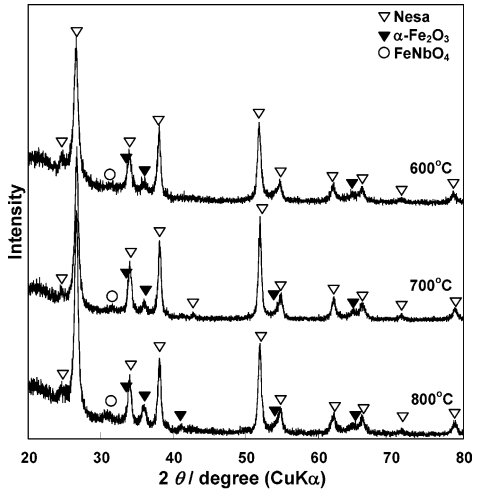

Figure 8. 8. XRD patterns of the film electrodes prepared from the solution of Nb/(Fe + Nb) = 0.25 and fired at different temperatures via three-times coating.

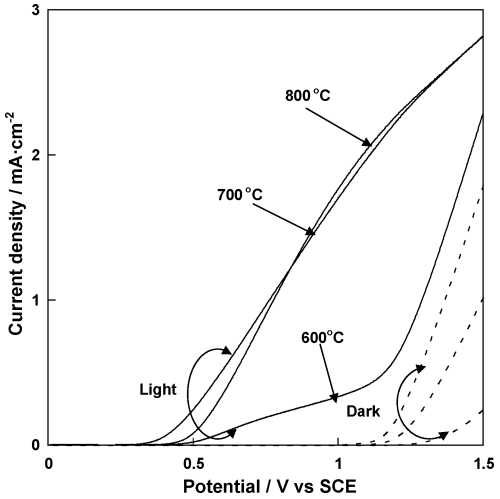

Figure 9. 9. Current−potential curves of the film electrodes prepared from the solution of Nb/(Fe + Nb) = 0.25 and fired at different temperatures via three-times coating.

observed in all the films. The α-Fe_2O_3 (110) peak ($2\theta = 35.6°$) increased slightly in intensity with increasing heating temperature.

Figure 9 shows the current−potential curves of these films. The photocurrent was the smallest for the film heated at 600 °C and almost the same for those heated between 700 and 800 °C. Figure 10 shows the action spectra of the films where the measurement was performed at a potential of 1 V vs SCE. Although the film heated at 600 °C showed photoresponse at wavelengths of <500 nm, the maximum IPCE was less than 1%. On the other hand, the films heated at 700 and 800 °C exhibited photoresponse extended to wavelengths around 600 nm and a remarkable increase in IPCE.

4. Discussion

4.1. Effect of Nb/(Fe + Nb) Ratio. When the Nb/(Fe + Nb) ratio increased from 0 to 0.25, the photocurrent under white light illumination increased for the films fired at 700 °C with three-times coating (Figure 4). When the Nb/(Fe + Nb) ratio was over 0.25, however, the photocurrent decreased. In the action spectra measured at 1 V vs SCE (Figure 5), when the Nb/(Fe + Nb) ratio increased from 0 to 0.25, IPCE increased both in the visible and UV regions, and the photoresponse

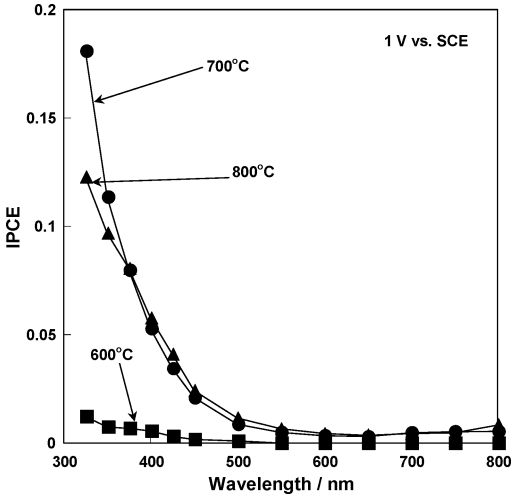

Figure 10. 10. Action spectra of the film electrodes prepared from the solution of Nb/(Fe + Nb) = 0.25 and fired at different temperatures via three-times coating. The measurement was conducted at 1.0 V vs SCE.

extended from 500 to 600 nm. When the Nb/(Fe + Nb) ratio increased over 0.25, IPCE decreased, while it increased again at wavelengths of <360 nm when the Nb/(Fe + Nb) ratio increased from 0.75 to 1. These indicate that the increase and decrease of the photocurrent with the Nb/(Fe + Nb) ratio increasing from 0 to 0.25 and over 0.25, respectively, are due to the variation of IPCE both in the visible and UV ranges.

When Figures 4 and 5 are compared in more detail, Nb0 exhibited a larger photocurrent than Nb0.5 under white light illumination (Figure 4), although Nb0 showed lower IPCE than Nb0.5 in the action spectra (Figure 5). This apparent discrepancy may come from the difference in light-intensity dependence of photocurrent between different Nb/(Fe + Nb) ratios: in $I-V$ curve measurements under white light, the light intensity was ca. 3 W at a wavelength of 500 nm, while in the action spectra measurement, the illuminating light had a much lower intensity of ca. 22 μW at the same wavelength.

4.1.1. Change in Photoanodic Properties with Increasing Nb/(Fe + Nb) Ratio from 0 to 0.25. Nb0 and Nb0.25 comprised single-phase α-Fe_2O_3 and coexisting phases α-Fe_2O_3 and $FeNbO_4$, respectively (Figure 1). The direct and indirect band gaps of α-Fe_2O_3 are 2.7 eV (460 nm) and 2.2 eV (560 nm),[6] respectively, while $FeNbO_4$ has 4.4 eV (280 nm) direct and 2.6 eV (480 nm) indirect band gaps.[9] The optical absorption spectra of Nb0 and Nb0.25 also reveal a larger band gap for $FeNbO_4$ than for α-Fe_2O_3; Nb0 has the absorption onset at a longer wavelength than Nb0.5. It should be noted that Nb0 (α-Fe_2O_3) has low absorbance in the UV range, whereas Nb0.25 (α-Fe_2O_3 + $FeNbO_4$) has high absorbance in the UV range due to $FeNbO_4$. It is then considered that the remarkable increase in IPCE observed in Nb0.25 in the UV range is due to the $FeNbO_4$ phase, which increases the number of photoexcited electrons in the UV range.

Then, why does IPCE increase in the visible range with the photoresponse extended to longer wavelengths, although the absorbance in the visible range shows negligible change when the Nb/(Fe + Nb) ratio increased from 0 to 0.25? As seen in Table 3, when the Nb/(Fe + Nb) ratio increased from 0 to 0.25, the donor density increased by 2−3 orders of magnitude. The increase in donor density is caused by Nb^{5+} doping in α-Fe_2O_3 as well as by $FeNbO_4$, which has high donor density (Table 3). The increase in donor density reduces the resistivity of the film,

resulting in the increase in IPCE in the visible range as well as in the UV range.

As seen in Figure 6, a spikelike transient response on chopping the light decreased with increasing Nb/(Fe + Nb) ratios from 0 to 0.25, and disappeared at Nb/(Fe + Nb) ratios over 0.5. The spikelike transient response results from the recombination of electrons and holes at the surface states.[12−14] Accordingly, when the Nb/(Fe + Nb) ratio increases from 0 to 0.25, the recombination of electrons and holes at the electrode surface is suppressed, which also contributes to the increase in IPCE. Because the spikelike transient response disappeared for Nb0.5 ($FeNbO_4$), $FeNbO_4$ crystals on the Nb0.25 surface are considered to contribute to the suppression of the electron/hole recombination.

SEM observation revealed that the size of the secondary particles increases when the Nb/(Fe + Nb) ratio increases from 0 to 0.25. The roughness of the surface also appears to be increased (Figure 2a,b). Although both particle size and surface roughness could affect the photoanodic properties, how they actually affect the properties is unknown.

4.1.2. Change in Photoanodic Properties with Increasing Nb/(Fe + Nb) Ratio over 0.25. When the Nb/(Fe + Nb) ratio increased from 0.25 to 0.5, the crystalline phases changed from $FeNbO_4$ + α-Fe_2O_3 to $FeNbO_4$, and the photocurrent under white light illumination (Figure 4) and IPCE in the action spectra (Figure 5) decreased, although the donor density rather increased (Table 3) and the spikelike photocurrent transient response disappeared. This is thought to be caused by the decrease in the number of photoexcited electrons in the visible range due to the absence of an α-Fe_2O_3 phase, as is revealed in the optical absorption spectra (Figure 3).

When the Nb/(Fe + Nb) ratio increased further from 0.5 to 0.75 and to 1, the crystalline phases changed from $FeNbO_4$ to $FeNbO_4$ + Nb_2O_5 and to Nb_2O_5, where the donor density (Table 3) and the onset wavelength of the absorption (Figure 3) decreased. The shift of the optical absorption to the shorter wavelengths is due to Nb_2O_5, which has a wide band gap of 3.4 eV, 360 nm.[15,16] The decrease in IPCE in the action spectra and the photocurrent under white light illumination is then attributed to the decrease in the absorption onset wavelength and donor density.

4.2. Effect of the Firing Temperature. For Nb0.25 with three-times coating, the photocurrent under white light illumination and IPCE under monochromatized light illumination remarkably increased when the firing temperature was raised from 600 to 700 °C. As seen in the XRD patterns (Figure 8), Nb0.25 samples consisted of α-Fe_2O_3 and $FeNbO_4$ phases when fired at 600, 700, or 800 °C. The XRD patterns revealed that crystallization proceeds with increasing firing temperature, especially as seen in the peak intensity of α-Fe_2O_3 (110) (2θ = 35.6°). Therefore, the increase in IPCE and photocurrent with increasing firing temperature results from the increase in crystallinity.

5. Conclusions

Sol−gel derived Fe_2O_3−Nb_2O_5 films were prepared from the solutions of various Nb/(Fe + Nb) mole ratios. The thicknesses of the single-layer films were 14−30 nm, while those of the films prepared with three-times coating were estimated to be 42−90 nm. The photoanodic properties of the films were studied in a wet cell.

When the Nb/(Fe + Nb) mole ratio increased from 0 to 0.25, the crystalline phases changed from α-Fe_2O_3 to α-Fe_2O_3 + $FeNbO_4$, the photoanodic current under white light illumination increased, and the photoanodic current under monochromatized light illumination increased both in the visible and UV ranges. The photoresponse extended to 600 nm, and IPCE was the maximum (18%) at the wavelength of 325 nm for the sample consisting of α-Fe_2O_3 and $FeNbO_4$ (Nb/(Fe + Nb) = 0.25). On the other hand, when the Nb/(Fe + Nb) ratio increased over 0.25, the crystalline phases changed to $FeNbO_4$, $FeNbO_4$ + Nb_2O_5, and Nb_2O_5, and the photoanodic current decreased. The highest IPCE in the visible and UV ranges observed for the sample of Nb/(Fe + Nb) = 0.25 results from the absorption in the visible range due to the α-Fe_2O_3 phase and the high donor density provided by the $FeNbO_4$ phase, as well as by the Nb^{5+}-doping in α-Fe_2O_3.

Acknowledgment. H. Kozuka thanks the High Technology Research Center of Kansai University for their financial support.

References and Notes

(1) Fujishima, A.; Honda, K.; Kikuchi, S. *Bull. Chem. Soc. Jpn.* **1969**, *72*, 108.

(2) Lindgren, T.; Wang, H.; Beermann, N.; Vayssieres, L.; Hagfeldt, A.; Lindquist, S.-E. *Sol. Energy Mater. Sol. Cells* **2002**, *71*, 231.

(3) Shinar, R.; Kennedy, J. H. *Sol. Energy Mater*. **1982**, *6*, 323.

(4) Dwight, K.; Wold, A. *ACS Symp. Ser.* **1981**, *146*, 207.

(5) Khan, S. U. M.; Zhou, Z. Y. *J. Phys. Chem. B* **1999**, *103*, 7184.

(6) Anderman, M.; Kennedy, J. H.; In *Semiconductor Electrodes*; Finklea, H. O., Ed.; Elesvier: New York, 1988; Chapter 3.

(7) Houlihan, J. F.; Pannaparayil, T.; Burdette, H. L.; Madacsi, D. P.; Pollock, R. J. *Mater. Res. Bull.* **1984**, *20*, 163.

(8) Okubayashi, M.; Kozuka, H. In Proceedings of the 2nd National Institute for Materials Science International Conference on Photocatalysis: Fundamentals and Applications; Feb. 1−3, 2004, Kanagawa; pp 89−92.

(9) Koenitzer, J.; Khazai, B.; Hormadaly, J.; Kershaw, R.; Dwight, K.; Wold, A. *J. Solid State Chem.* **1980**, *35*, 128.

(10) Wilhelm, S. M.; Yun, K. S.; Ballenger, L. W.; Hackerman, N. *J. Electrochem. Soc.* **1979**, *126*, 419.

(11) Fain Seramikkusu Jiten (Fine Ceramics Dictionary); Fain Seramikkusu Jiten Henshu Iinkai (Editorial Board of Fine Ceramics Dictionary), Eds.; Gihoudou Publishing Co.: Japan, 1987; p 295 (in Japanese).

(12) Iwanski, P.; Curran, J. S.; Gissler, W. *J. Electrochem. Soc.* **1981**, *128*, 2128.

(13) Watanbe, A.; Kozuka, H. *J. Phys. Chem. B* **2003**, *107*, 12713.

(14) Benko, F. A.; Longo, J.; Koffyberg, F. P. *J. Electrochem. Soc.* **1985**, *132*, 609.

(15) Chen, S. G.; Chappel, S.; Diamant, Y.; Zaban, A. *Chem. Mater*. **2001**, *13*, 4629.

(16) De A. Barros, D. F. O.; Abreu, P. P. F. O.; Werner, U.; Aegerter, M. A. *J. Sol-Gel Sci. Technol.* **1997**, *18*, 735.